Spring 1998

A Study of the Volume of Fluid Method for Moving Boundary Problems

Marianne Francois
Embry-Riddle Aeronautical University - Daytona Beach

A STUDY OF THE VOLUME OF FLUID METHOD FOR MOVING BOUNDARY PROBLEMS

by

Marianne François

A Thesis Submitted to the Graduate Studies Office in Partial Fulfillment of the Requirements for the Degree of Master of Science in Aerospace Engineering

Embry-Riddle Aeronautical University
Daytona Beach, Florida
Spring 1998

A STUDY OF THE VOLUME OF FLUID METHOD FOR MOVING BOUNDARY PROBLEMS

by

Marianne François

This thesis was prepared under the direction of the candidate's thesis committee chairmen, Dr. Wei Shyy, Departement of Aerospace Engineering, Mechanics and Engineering Science at University of Florida, and Dr. David Kim, Departement of Aerospace Engineering at Embry Riddle, and has been approved by the members of his thesis committee. It was submitted to the Office of Graduate Studies and was accepted in partial fulfillment of the requirements for the degree of Master of Science in Aerospace Engineering.

THESIS COMMITTEE:

Dr. Wei Shyy
Chairman

Dr. David Kim
Co-Chairman

Dr. Tej R. Gupta
Member

Dr. Lakshmanan Narayanaswami 4/23/98
Member

Dr. Allen I. Ormsbee
Department Chairman, Aerospace Engineering

Date: 5/5/98

ACKNOWLEDGMENTS

I would like to express my gratitude to the individuals who have helped me accomplish this thesis.

My greatest appreciation and respect go to Dr. Wei Shyy, Chair of my committee, for his guidance, his encouragement, and his knowledge of the topics. Also, I would like to express my appreciation to Dr. Andrew Martin for his invaluable help with the code and for his patience.

I would like to give special thanks to Dr. David Kim, Co-Chair of my committee, who helped me to do my thesis in the field of "Fluid Physics in Microgravity" by making possible my work with University of Florida.

I would like to express my appreciation for the contributions made by my thesis committee members, Dr. Tej Gupta. and Dr. Narayananswami.

I would like to thank Alain Jeneveau, Erna Ortodoro, Dr. Ray Wimberly, and Judith Assad, who made possible my transfer for my graduate study from Ecole Polytechnique Feminine in Paris, to Embry-Riddle Aeronautical University. I also want to thank Monica Frappier of ERAU's Graduate Programs for her help in the paperwork administration.

This statememt of acknowlegement would be incomplete without expressing my sincere appreciation and gratitude to both my friends and family. I particularly thank my parents and my sister for their continuous support and encouragement.

ABSTRACT

Author: Marianne François
Title: A Study of the Volume of Fluid Method for Moving Boundary Problems
Institution: Embry Riddle Aeronautical University
Degree: Master of Science in Aerospace Engineering
Year: 1998

Moving boundary problems are often encountered in engineering and science. One of the methods to solve such problems numerically is the volume of fluid (VOF) method. The VOF method uses an additional field variable f to track the interface using the Eulerian fixed grid. In this work, the VOF method is combined with the Continuum surface force model. The governing flow equations for Newtonian fluids in incompressible flow in two dimensions are solved using the pressure-based algorithm. A linear interface reconstruction algorithm is developed and improved by interpolations. In order to validate the code, the problem of the convection of a two-fluid channel flow with a cylindrical interface is given as an example.

TABLE OF CONTENTS

LIST OF TABLES

LIST OF FIGURES

NOMENCLATURE

A	area formed by the interface in a cell
f	volume of fluid variable
$\vec{F}_{sv}$	surface tension volume force
$\vec{n}$	normal to the interface
p	pressure variable
R', R''	principal radii of curvature of the interface
S	source term
t	time
$\vec{V}$	velocity vector
u	x-component of the velocity
v	y-component of the velocity
V_n	normal velocity component

Greek

ρ	density
μ	viscosity
σ	surface tension
κ	curvature of the interface

ϕ	general flow variable
Γ	diffussion term

Subscripts

1	fluid 1
2	fluid 2
x	x-component
y	y-component
i	computational indice in x-direction
j	computational indice in y-direction

Dimensionless Coefficients

Re	Reynolds number	$\mathrm{Re} = \frac{\rho U L}{\mu}$
Ca	Capillary number	$Ca = \frac{\mu U}{\sigma}$

CHAPTER 1: INTRODUCTION

1.1 Motivation

Moving boundary problems are often encountered in multiphase flows. Multiphase flows are flows in which different physical phases (gas, liquid, and solid) coexist. Since multiphase flows are numerous in many engineering applications under earth gravity and in space applications, studies of numerical techniques for moving boundary problems are needed in order to perform better numerical simulation of the problem. Nowadays, moving boundary problems are also very important in microgravity science research. These applications in engineering and science include melting and solidification, crystal growth, flame propagation, pipeline transport of oil/natural gas mixtures, flows in nuclear reactor, evaporation and condensation, transfer line flows of cryogenic fluids, etc. Moving boundary problems are characterized by interfaces demarcating regions with different physico-chemical properties. Across these interfaces, compositions, phases, material properties and flow features can vary rapidly. Also, these interfaces move under the influence of the flow field and, in turn, affect the behavior of the flow. Due to the interaction of fluid flows with the interface which leads to a highly

coupled, nonlinear system, moving boundary problems are very difficult to analyze. The main difficulty is that the internal boundary position and shape must be determined as part of the solution of the transport equations of mass continuity, momentum, and energy. The interface is often treated as a discontinuity in the flow field which needs to be tracked accurately both in time and space, within the limitation of finite grid resolution. In the next paragraph, different numerical methods used to solve moving boundary problems are presented.

1.2 Numerical Methods Applied to General Moving Boundary Problems

There are several available techniques for tracking arbitrary interfaces, each with its own advantages and disadvantages (Floryan and Ramussen 1989, Shyy et al. 1996). These techniques are categorized as (a) surface tracking or Lagrangian methods, and (b) volume tracking or Eulerian methods. The main features of the two categories are presented in Figure 1.1.

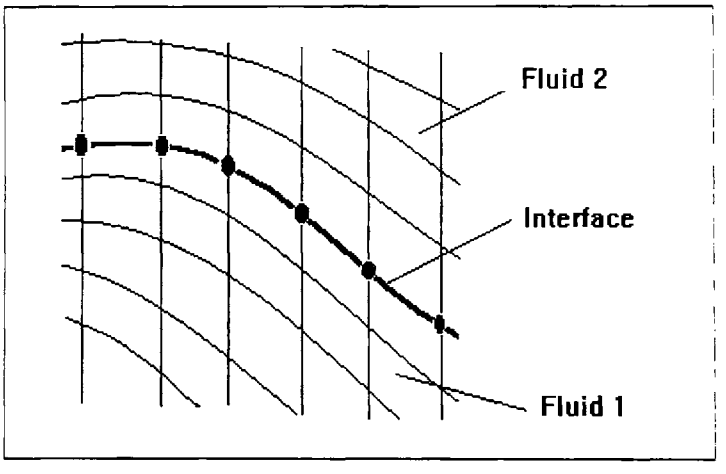

Figure 1.1.a: Lagrangian method with a moving, boundary conforming grid

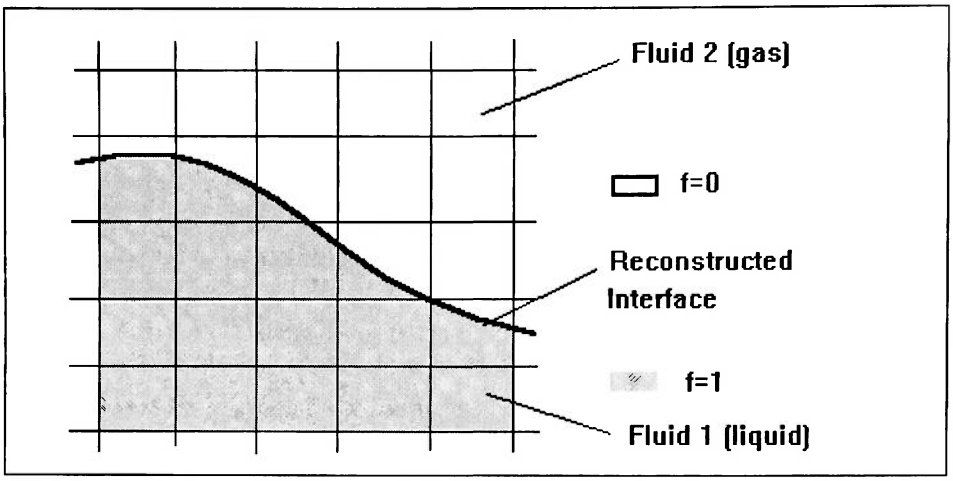

Figure 1.1.b: Fixed-grid Eulerian method with a phase fraction f definition of the interface

(a) Lagrangian Method

In the Lagrangian methods, the grid is configured to conform to the shape of the interface, and thus it adapts continually to it. The two main advantages of Lagrangian methods are: (i) the interface is explicitly tracked, (ii) the interfacial boundary conditions apply at the exact location of the interface. The main disadvantage with Lagrangian methods is the numerical inaccuracy due to the irregular grid.

(b) Eulerian Method

The Eulerian methods usually employ a fixed grid formulation, and the interface between the two phases is not explicitly tracked but is reconstructed from the properties of appropriate field variables, such as fluid fractions. Eulerian methods need procedures to deduce the interface location based on the volume fraction information. Also, the interfacial boundary conditions need to be manipulated to appear in the governing transport equations. The main advantage of the Eulerian is the good accuracy in the calculation of the field variables due to its fixed grid. The principal disadvantages of the

method are (i) the difficulty in calculating the position of the interface accurately, and (ii) the possible smearing of boundary information due to the manipulation of the interfacial boundary conditions.

The choice of a Lagrangian or Eulerian approach is dependent on the physical problem to be solved. If details of the interface are secondary and are unlikely to significantly impact the global flow features, Eulerian methods are more attractive. If the discontinuity across the interface is to be maintained with high fidelity, and if interfacial behavior is the focus, Lagrangian methods may be preferable. Furthermore, there are combined Eulerian-Lagrangian methods (Shyy et al. 1996) that have yielded solutions with combined characteristics of both Eulerian and Lagrangian methods.

1.3 The Volume of Fluid (VOF) method

The Volume of Fluid method (VOF) is a fixed-grid interface tracking method, more precisely, a volume-tracking (Eulerian) method. In volume-tracking methods, the interface is not explicitly defined or tracked but is reconstructed based on the information of the volume fraction of the fluid. The VOF method, pioneered by Hirt and Nichols (1981), is designed for two immiscible fluids, where the position of the interface between the fluid is of interest. In the VOF method a single set of momentum equations is shared by the fluids, and the volume fraction of each of the fluids is tracked throughout the domain. The basic idea is to define a liquid fraction variable field f, on an Eulerian fixed grid. In a grid cell $f=1$ if the cell is completely in liquid phase, $f=0$ if the cell is empty, and $0<f<1$ if the cell contains the interface. The volume fraction is then advected with the

local flow velocity. Over the years, more accurate schemes for advecting the volume fractions have been developed (Youngs 1984, Ashgriz and Poo 1991, Liang 1991, Brackbill et al. 1992, Kothe and Mjolness 1992). As reviewed by Kothe and Rider (1994), in general, two classes of algorithms have been employed, namely, piecewise constant and piecewise linear, yielding different degrees of accuracy, to recover the interface shape. The main disadvantage of the VOF is that the interface is not handled with precision. The difficulty arises in the interface reconstruction which involves a considerable amount of logical operations. Only recently has a technique, referred to as the Continuum Surface Force (CSF) model, been developed (Brackbill et al. 1992) to impose surface tension effects in an efficient manner. In this method, the boundary conditions on the interface are assigned in a weighted fashion to the computational nodes in the vicinity of the interface instead of being applied directly on the boundary. Volume tracking methods have been applied to complex interfacial phenomena. Applications of the VOF include the prediction of jet breakup (Liang, 1991, Kothe and Mjolness, 1992), the motion of large bubbles in a liquid (Tomiyama et al. 1996, and Mack et al. 1995), the motion of liquid after a dam break (Hirt and Nichols 1981), or the steady or transient tracking of any liquid-gas interface.

1.4 Overview of Present Work

In the present work the volume of fluid method is investigated for moving boundary problems. To this extent, a computational code has been developed in which the VOF method is combined with the CSF model and an interface reconstruction is

proposed. To limit the complexity of the problem, the present discussion is on Newtonian fluids, for incompressible flows only, and the transport equation of energy is not considered. The flow equations are solved in Cartesian coordinates in two dimensions by using Patankar's algorithm.

In Chapter 2 the governing equations and boundary conditions of the moving boundary problem are presented. The VOF method and the CSF model are described and the pressure-based algorithm of Patankar is reviewed.

In Chapter 3, an interface reconstruction algorithm is proposed. A piecewise linear approximation algorithm has been set up. From this approximation the accuracy is improved by interpolation.

In order to validate the code, Chapter 4 presents an example of a moving boundary problem: the translation of a spherical bubble in a channel.

This thesis ends with Chapter 5 which contains a conclusion of this work, and recommendations for future research efforts.

CHAPTER 2: NUMERICAL TECHNIQUES

In this chapter, the fundamental fluid dynamic conservation laws are presented for Newtonian fluids. The volume of fluid (VOF) method and the continuum surface force (CSF) model are described. A description of the pressure-based algorithm suitable for the Navier-Stokes and associated transport equations is given. The basic algorithm closely follows the original work of Patankar (1980) in Cartesian coordinates.

2.1 Formulation

2.1.1 General Governing Flow Equations

The governing equations in Cartesian cooordinates for two-dimensional, incompressible flow can be written in dimensional form as:

continuity

$$\frac{\partial \rho}{\partial t}+\frac{\partial(\rho u)}{\partial x}+\frac{\partial(\rho v)}{\partial y}=0 \tag{2.1.1}$$

x-momentum

$$\frac{\partial(\rho u)}{\partial t}+\frac{\partial(\rho u u)}{\partial x}+\frac{\partial(\rho u v)}{\partial y}=-\frac{\partial p}{\partial x}+\left[\frac{\partial}{\partial x}\left(\mu\frac{\partial u}{\partial x}\right)+\frac{\partial}{\partial y}\left(\mu\frac{\partial u}{\partial y}\right)\right]+S_u \tag{2.1.2}$$

y-momentum

$$\frac{\partial(\rho v)}{\partial t}+\frac{\partial(\rho uv)}{\partial x}+\frac{\partial(\rho vv)}{\partial y}=-\frac{\partial p}{\partial y}+\left[\frac{\partial}{\partial x}\left(\mu\frac{\partial v}{\partial x}\right)+\frac{\partial}{\partial y}\left(\mu\frac{\partial v}{\partial y}\right)\right]+S_v \tag{2.1.3}$$

where ρ is the fluid density, u is the fluid velocity component in the x-direction, v is the fluid velocity component in the y-direction, p is the pressure and μ is the viscosity. S_u, S_v are the source terms which include, the gravity term and the surface tension contribution. They will be described later.

2.1.2 Boundary Conditions at the Interface

The interface is regarded as a free surface of constant pressure without shear stress. The boundary conditions to be applied on the interface for cases involving no mass exchange across it are the continuity condition and normal stress balance:

$$(V_n)_1=(V_n)_2=(V_n)_I \tag{2.1.4}$$

$$p_2-p_1=\sigma\kappa+2\mu_2\left(\frac{\partial V_n}{\partial n}\right)_2-2\mu_1\left(\frac{\partial V_n}{\partial n}\right)_1 \tag{2.1.5}$$

where subscripts 1 and 2 denotes the two fluids (fluid 1 and fluid 2), I represents the interface, σ is the surface tension, p is the pressure, and V_n is the normal velocity component, with the normal pointing from fluid 2 into fluid 1, as shown in Figure 2.1.

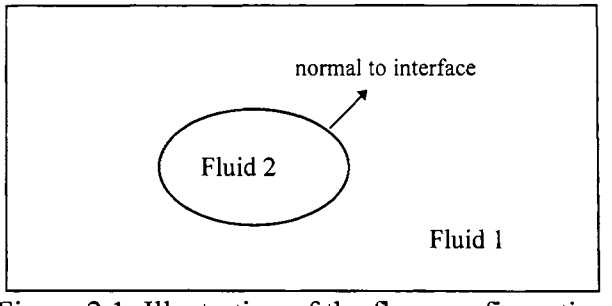

Figure 2.1: Illustration of the flow configuration

And where the curvature κ is defined as

$$\kappa = \left(\frac{1}{R'} + \frac{1}{R''} \right) \tag{2.1.6}$$

where R' and R'' are the local principal radii of curvature at the bubble surface.

2.2 Theory of the VOF Method

In the Volume of Fluid method, the free surface is treated by introducing a function $f(x,y,t)$ that is defined to be unity at any point occupied by the fluid and zero elsewhere. When averaged over a cell of the computating mesh, $f_{i,j}$ is the fractional volume of the cell i,j occupied by fluid. Thus, if $f_{i,j}=1$ the cell i,j is full of fluid, and if $f_{i,j}=0$ the cell i,j is empty of fluid. When $0<f_{i,j}<1$ the cell i,j is partially filled with fluid , thus it contains the interface. The governing equation for f, referred to the volume fraction equation is:

$$\frac{\partial f}{\partial t} + \frac{\partial (f u)}{\partial x} + \frac{\partial (f v)}{\partial y} = 0 \tag{2.2.1}$$

where the initial condition, i.e., $f(x,y,0)$ is given by initializing the free surface geometry. The above equation states that f moves with the fluid in time and space. Numerical solution of this equation for f, gives $f_{i,j}$ directly. The VOF method requires only one storage variable for each mesh cell to define the interface. The detailed shape is then processed after f is computed. In an Eulerian calculation, it is necessary to compute the flow of fluid through the mesh, which requires an averaging of the flow properties. Thus, the density and viscosity are averaged as follows:

$$\rho_{i,j} = \rho_{liq} f_{i,j} + \rho_{gas}(1 - f_{i,j}) \tag{2.2.2}$$

$$\mu_{i,j} = \mu_{liq} f_{i,j} + \mu_{gas}(1 - f_{i,j}) \tag{2.2.3}$$

Gradients of f determine the normal to the interface, and, together with f values, permit construction of an approximate interface. The procedure of the interface reconstruction is discussed in Chapter 3.

2.3 The Continuum Surface Force (CSF) Method

2.3.1 Theory

The Continuum Surface Force model was developed by Brackbill et al. 1992. In the CSF model, surface tension is modeled as a volume force.

The viscous effect terms at the interface are neglected and the surface tension σ is assumed to be constant, thus the normal stress equation Eq. (2.1.5) is reduced to Laplace's formula:

$$p_2 - p_1 = \sigma\kappa \tag{2.3.1}$$

where p_1 and p_2 are the pressures of fluid 1 and 2 respectively, and κ the mean free-surface curvature, given by:

$$\kappa = -\frac{1}{\|\vec{n}\|}\left(\nabla \cdot \vec{n}\right) \tag{2.3.2}$$

where $\vec{n}$ is the normal vector to the interface and defined as $\vec{n} = \nabla f$, the gradient of the VOF function. Hence,

$$\vec{n} = \left(\frac{\partial f}{\partial x}, \frac{\partial f}{\partial y} \right) \tag{2.3.3}$$

$$\kappa = -\frac{1}{\|\vec{n}\|} \nabla^2 f = -\frac{1}{\|\vec{n}\|} \left(\frac{\partial^2 f}{\partial x^2} + \frac{\partial^2 f}{\partial y^2} \right) \tag{2.3.4}$$

Because the curvature is proportional to the second derivatives of the VOF function (Eq. 2.3.4), surface force modeling is extraordinarily sensitive to small errors in *f*.

In the CSF model, the surface tension is reformulated as a volume force $\vec{F}_{sv}$. within free surfaces, i.e. at cells where $0<f<1$. The volume force is given by:

$$\vec{F}_{sv} = \sigma \kappa \nabla f \tag{2.3.5}$$

$$F_{sv/x} = \sigma \kappa \frac{\partial f}{\partial x} \tag{2.3.5.a}$$

$$F_{sv/y} = \sigma \kappa \frac{\partial f}{\partial y} \tag{2.3.5.b}$$

where $F_{sv/x}$ and $F_{sv/y}$ are the x and y components of $\vec{F}_{sv}$, respectively.

Surface tension effects at free surfaces are modeled by the volume force $\vec{F}_{sv}$ as a body force in the momentum transport equation in addition, of course, to other arbitrary body forces present in the flow. If there were no arbitrary body force in the flow, S_u and S_v will be simply equal to $F_{sv/x}$ and $F_{sv/y}$. In this model, surface tension acts everywhere within the transition region through the volume force $\vec{F}_{sv}$.

2.3.2 Calculation of the Normal Vector $\vec{n} = (n_x, n_y)$

$$\boxed{\vec{n} = \nabla f} \quad \Rightarrow \quad n_x = \frac{\partial f}{\partial x} \qquad n_y = \frac{\partial f}{\partial y}$$

The normal vector components are computed at the four vertices of the cell (at en, wn, ws, es). And the cell-centered normal is the average of the vertex normals.

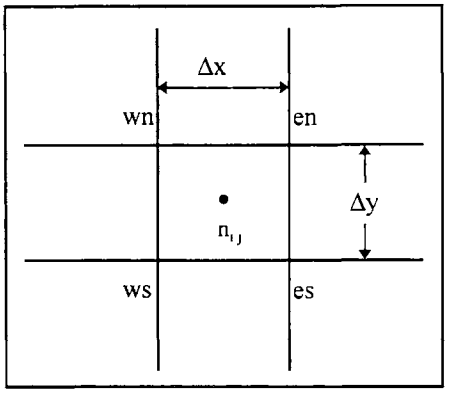

Figure 2.2: Schematic of the cell

$$n_{xen} = \frac{(f_{i+1,j+1} - f_{i,j+1}) + (f_{i+1,j} - f_{i,j})}{2\Delta x} \qquad n_{xes} = \frac{(f_{i+1,j} - f_{i,j}) + (f_{i+1,j-1} - f_{i,j-1})}{2\Delta x}$$

$$n_{xwn} = \frac{(f_{i,j+1} - f_{i-1,j+1}) + (f_{i,j} - f_{i-1,j})}{2\Delta x} \qquad n_{xws} = \frac{(f_{i,j} - f_{i-1,j}) + (f_{i,j-1} - f_{i-1,j-1})}{2\Delta x}$$

$$n_x = \frac{1}{4}(n_{xen} + n_{xes} + n_{xwn} + n_{xws}) \tag{2.3.6}$$

$$n_{yen} = \frac{(f_{i+1,j+1} - f_{i+1,j}) + (f_{i,j+1} - f_{i,j})}{2\Delta y} \qquad n_{yes} = \frac{(f_{i+1,j} - f_{i+1,j-1}) + (f_{i,j} - f_{i,j-1})}{2\Delta y}$$

$$n_{ywn} = \frac{(f_{i,j+1} - f_{i,j}) + (f_{i-1,j+1} - f_{i-1,j})}{2\Delta y} \qquad n_{yws} = \frac{(f_{i,j} - f_{i,j-1}) + (f_{i-1,j} - f_{i-1,j-1})}{2\Delta y}$$

$$n_y = \frac{1}{4}(n_{yen} + n_{yes} + n_{ywn} + n_{yws}) \tag{2.3.7}$$

$$\|\vec{n}\| = \sqrt{n_x^2 + n_y^2} \tag{2.3.8}$$

2.3.3 Calculation of the Curvature κ

The curvature is defined by $\kappa = -\frac{1}{\|\vec{n}\|}(\nabla \cdot \vec{n})$ (2.3.9)

$$\text{or } \kappa = -\frac{1}{\|\vec{n}\|}\left(\frac{\partial n_x}{\partial x} + \frac{\partial n_y}{\partial y}\right) \tag{2.3.10}$$

with $$\frac{\partial n_x}{\partial x} = \frac{1}{2\Delta x}(n_{xen} - n_{xwn} + n_{xes} - n_{xws}) \tag{2.3.11}$$

and $$\frac{\partial n_y}{\partial y} = \frac{1}{2\Delta y}(n_{yen} - n_{ywn} + n_{yes} - n_{yws}) \tag{2.3.12}$$

2.3.4 Calculation of the Surface Force

$$\vec{F}_{sv/x} = \sigma\kappa n_x \tag{2.3.13.a}$$

$$\vec{F}_{sv/y} = \sigma\kappa n_y \tag{2.3.13.b}$$

2.4 Discretization of the Flow Equations: Patankar's Algorithm

The discretization of the governing equation is carried out using a control volume formulation. The differential equation is integrated over each control volume. The general differential equation for a convection-diffusion problem, for the general variable ϕ, can be written in a conservative form as

$$\frac{\partial}{\partial t}(\rho\phi)+\frac{\partial}{\partial x_j}(\rho u_j\phi)=\frac{\partial}{\partial x_j}\left(\Gamma\frac{\partial\phi}{\partial x_j}\right)+S \qquad (2.4.1)$$

where ρ is the density, u_j the jth component of the velocity, Γ the diffusion coefficient, and S the source term for the variable ϕ. The finite volume formulation is adopted; hence the two-dimensional form of Eq. (2.4.1) can be written as

$$\frac{\partial}{\partial t}(\rho\phi)+\frac{\partial J_x}{\partial x}+\frac{\partial J_y}{\partial y}=S \qquad (2.4.2)$$

where J_x and J_y are the total (convection plus diffusion) fluxes defined by

$$J_x \equiv \rho u\phi-\Gamma\frac{\partial\phi}{\partial x} \quad , \quad J_y \equiv \rho v\phi-\Gamma\frac{\partial\phi}{\partial y} \qquad (2.4.3)$$

where u, v are the velocity components in the x and y directions, respectively.

In the case of the continuity equation, ϕ is equal to 1, and Γ=0 In the case of the x and y-momentum equation, ϕ is equal to u and v, respectively, and $\Gamma=\mu$. And, in the case of the fluid fraction equation, ϕ is equal to f, ρ =1 and Γ=0.

The SIMPLE algorithm of Patankar with a uniform grid is adopted as the computational algorithm. Following the notation of Patankar, for two-dimensional problems, the discrete equation is the following:

$$a_P\phi_P=a_I\phi_I+a_W\phi_W+a_N\phi_N+a_S\phi_S+b \qquad (2.4.4)$$

where a_P is the coefficient of the variable at the grid point under consideration and a_I, a_W, a_N, a_S are the coefficients of the four immediate neighbors. The term b is referred to as the source term and contains the explicit source terms as well as the terms involving the grid points other than the five points mentionned earlier.

The quantities S_C and S_P arise from the source term linearization of the form

$$S = S_c + S_P \phi_P \tag{2.4.5}$$

Figure 2.3 gives a schematic explanation of the symbols used.

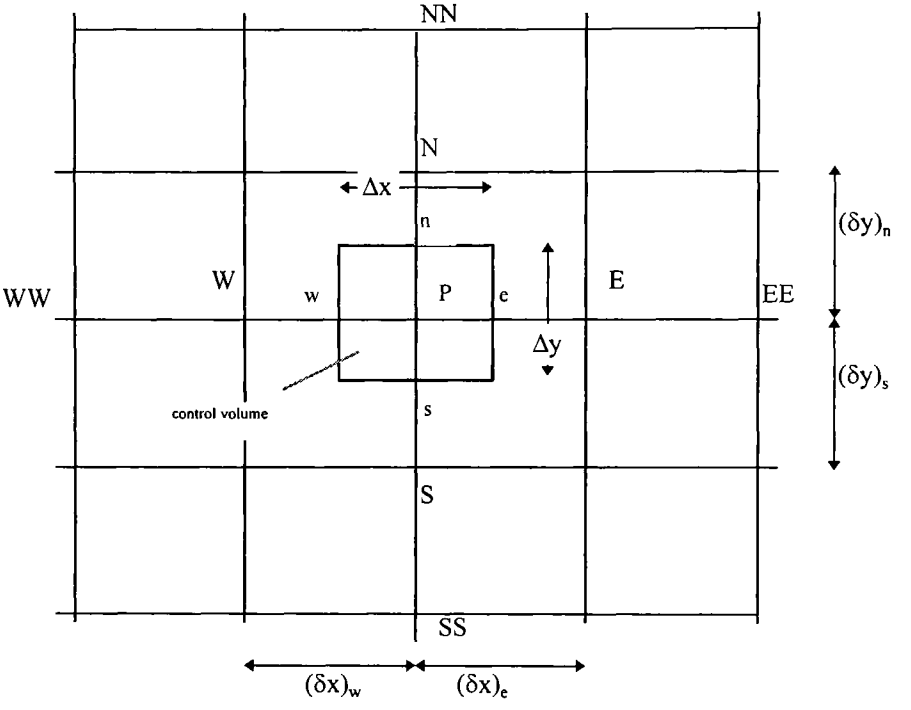

Figure 2.3: Schematic of the control volume

The coefficients for the final discretization equation with central difference operator for convections terms are given by

$$a_E = D_e A(|P_e|) + \max[-F_e, 0] \tag{2.4.6.a}$$

$$a_W = D_w A(|P_w|) + \max[F_w, 0] \tag{2.4.6.b}$$

$$a_N = D_n A(|P_n|) + \max[-F_n, 0] \tag{2.4.6.c}$$

$$a_S = D_s A(|P_s|) + \max[F_s, 0] \tag{2.4.6.d}$$

$$a_P^0 = \frac{\rho_P^0 \Delta x \Delta y}{\Delta t} \tag{2.4.6.e}$$

$$b = S_C \Delta x \Delta y + a_P^0 \phi_P^0 \tag{2.4.6.f}$$

$$a_p = a_E + a_W + a_N + a_S + a_P^0 - S_P \Delta x \Delta y \tag{2.4.6.g}$$

Here, ϕ_P^0 and ρ_P^0 refer to the known values at time t, while all other values $(\phi_P, \phi_E, \phi_N, \phi_S)$ and so on, are the unknown values at time t+Δt.

The neighbor coefficients a_E, a_W, a_N, a_S represent the convection and diffusion influence at the four faces of the control volume, in terms of the flow rate F and the conductance D.

The conductance terms have been represented by the standard second-order central difference scheme. The coefficients for the diffusion fluxes are the following:

$$D_e = \frac{\Gamma_e \Delta y}{(\delta x)_e} \tag{2.4.7.a}$$

$$D_w = \frac{\Gamma_w \Delta y}{(\delta x)_w} \tag{2.4.7.b}$$

$$D_n = \frac{\Gamma_n \Delta x}{(\delta y)_n} \tag{2.4.7.c}$$

$$D_s = \frac{\Gamma_s \Delta x}{(\delta y)_s} \tag{2.4.7.d}$$

where *e, w, n* and *s* designate the location of the control surface of each control volume. The mass fluxes F across each control surface are given by

$$F_e = (\rho u)_e \Delta y \tag{2.4.8.a}$$

$$F_w = (\rho u)_w \Delta y \tag{2.4.8.b}$$

$$F_n = (\rho v)_n \Delta x \tag{2.4.8.c}$$

$$F_s = (\rho v)_s \Delta x \tag{2.4.8.d}$$

and the cell Peclet numbers P are given by

$$P_e = \frac{F_e}{D_e} \tag{2.4.9.a}$$

$$P_w = \frac{F_w}{D_w} \tag{2.4.9.b}$$

$$P_n = \frac{F_n}{D_n} \tag{2.4.9.c}$$

$$P_s = \frac{F_s}{D_s} \tag{2.4.9.d}$$

And, the function A is defined as

$$A(|P|) = 1 - 0.5|P| \tag{2.4.10}$$

CHAPTER 3: INTERFACE RECONSTRUCTION

The problem is to reconstruct the interface given only the grid and the volume of fluid fraction $f_{i,j}$. For solving this problem a volume of fluid interface reconstruction algorithm has been set up and is described in this chapter. This algorithm gives a linear approximation to the interface in each cell where $0<f_{i,j}<1$ by considering the volume of fluid fraction in a 3x3 block of cells. This linear approximation is then improved.

1	1	1	0.9	0.3
1	1	1	0.6	0
1	1	0.8	0.1	0
1	0.9	0.2	0	0
1	0.4	0	0	0

Figure 3.1: Example of a volume of fluid fraction distribution in a fixed grid

3.1 Previous Work

Hirt and Nichols (1981) represented the interface by a set of horizontal or vertical lines (Figure 3.2.b). Youngs (1982) (Figure 3.2.c) determined the interface by using the volume of fluid fractions for the cell under consideration and its eight surrounding cells

but neither did he present the details of his technique for calculating the surface slope nor the procedure to detect the different cases. The Ashgriz and Poo (1991) method is to find the slope of the line segment based only on two neighboring volume fractions. In their technique the line segments are drawn at the cell boundaries (Figure 3.2.d).

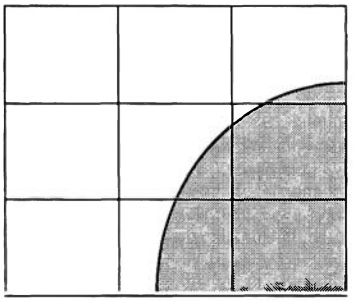

(a) actual surface

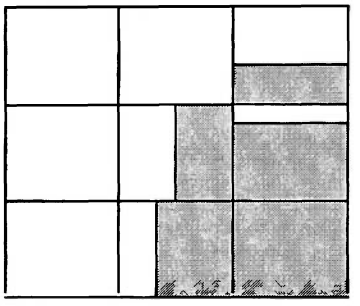

(b) Hirt and Nichols (1981)

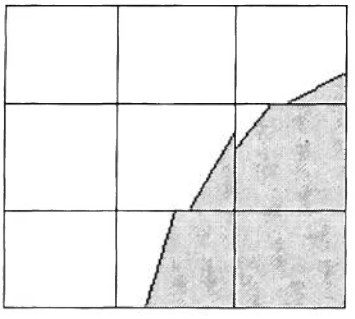

(c) Youngs (1982)

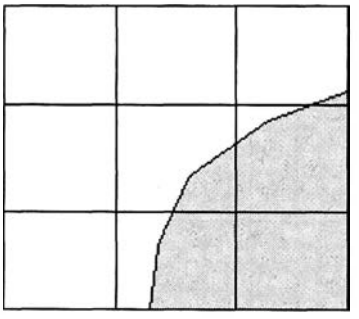

(d) Ashgriz and Poo (1991)

Figure 3.2: Comparisons of the previous interface representation techniques

3.2 Piecewise Linear Approximation

3.2.1 General Description

In this work a piecewise linear approximation algorithm is set up. The interface reconstruction takes place in the cells where $0 < f_{i,j} < 1$. Piecewise linear approximations are not continuous. A 3 x 3 block of cells is considered to determine the approximate interface in the center cell of the block. First, the normal vector $\vec{n}_{i,j}$ is calculated at the cell-centered. The calculation of the normal vector is presented in paragraph 2.3.2. The normal vector gives the direction of the interface. Let the interface equation be the line:

$$n_x x + n_y y = d \tag{3.1.1}$$

where n_x is the x-component, n_y is the y-component of the normal vector and where d defines the position of the line to the origin. The position of the line interface is adjusted to match the volume of fluid $f_{i,j}$. The line (interface) intersects the grid at two locations: point1(*xin1*, *yin1*) and point2(*xin2*, *yin2*). Once these 2 points are found, the line (interface) is defined. When all the intersection points of the interface with the grid are computed, the interface can be plotted.

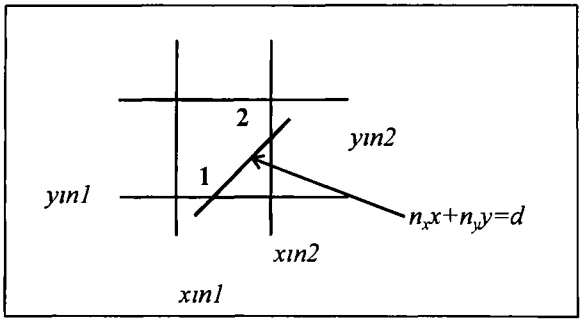

Figure 3.3: Illustration of an interface intersecting two cell sides.

The interface can intersect:

- adjacent sides (south-east, north-east, north-west, south-west) or

- opposite sides (west-east, north-south).

To know which case is to apply, the f values in the surrounding cells are tested. For each case a detailed description is presented in the following paragraphs.

3.2.2 Case of the Interface Intersecting Adjacent Sides

The interface intersects adjacents sides, if it intersects the southern and eastern sides of the cell under consideration, or northern and eastern sides, or northern and western sides, or finally, southern and western sides. In the case where the interface intersects adjacent sides, the interface line with the grid forms a triangular area. The base of the triangle is denoted by b, and the height by h. The area of a cell is $dxdy$. The different cases are detected by testing the f values in the surrounding cells. Values of f are written in each sketch cases.

(a) case south-east

The interface intersects the southern side at $yin1 = y_{j-1}$, and the interface cuts the eastern side at $xin2 = x_i$. The interface line must pass through the two points of intersection, so

$$n_x x_i + n_y yin2 = d \qquad (3.2.1.a)$$

$$n_x xin1 + n_y y_{j-1} = d \qquad (3.2.1.b)$$

(3.1.2.a)-(3.1.2.b): $$n_x(x_i - xin1) + n_y(yin2 - y_{j-1}) = 0 \qquad (3.2.2)$$

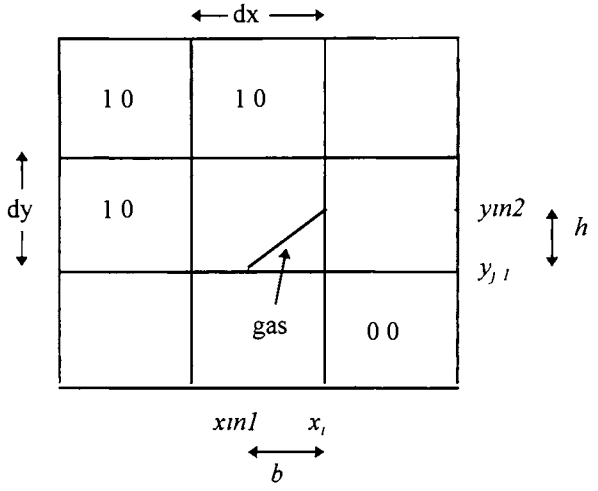

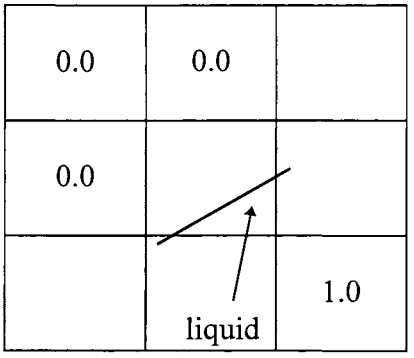

Figure 3.4: Illustration of interface intersecting south and east sides

Let $b = x_I - xin1$ and $h = yin2 - y_{J-1}$,

Thus Eq. (3.2.2) becomes:

$$n_x b + n_y h = 0 \qquad (3.2.3)$$

Let A be the area of the triangle formed by the interface intersecting the southern and eastern sides:

$$A = \frac{b \cdot h}{2} \qquad (3.2.4)$$

where $A = (1 - f_{i,j})\,dx\,dy$ for gas (3.2.5.a)

and $A = f_{i,j}\,dx\,dy$ for liquid (3.2.5.b)

By solving Eq. (3.1.4) with Eq. (3.1.5), h and b are found.

$$h = \sqrt{-2\frac{n_x}{n_y}A} \tag{3.2.6}$$

$$b = -\frac{n_y}{n_x}h \tag{3.2.7}$$

And finally, $xin1 = x_i - b$ and $yin2 = y = y_{j-1} + h$

In a the same way, the intersection points are determined for the cases where the interface intersects north-east, north-west, and south east sides.

(b) case north east

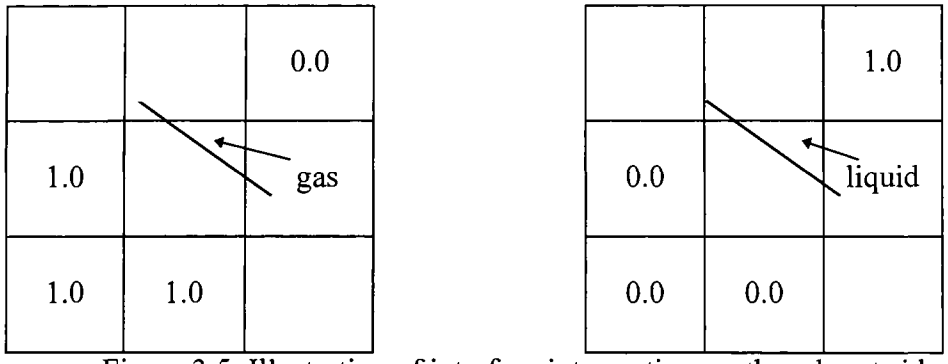

Figure 3.5: Illustration of interface intersecting north and east sides

$$n_x x_i + n_y y = d \tag{3.2.8.a}$$

$$n_x x + n_y y_j = d \tag{3.2.8.b}$$

(3.1.8.a)-(3.1.8.b): $n_x(x_i - x) + n_y(y - y_j) = 0$ (3.2.9)

Let $b = x_i - x$ and $h = y_j - y$,

Thus, $n_x b - n_y h = 0$ (3.2.10)

$$\frac{b \cdot h}{2} = A \qquad (3.2.11)$$

where $A = (1 - f_{i,j})\,dx\,dy$ for gas (3.2.12.a)

and $A = f_{i,j}\,dx\,dy$ for liquid (3.2.12.b)

$$h = \sqrt{2\frac{n_x}{n_y}A} \qquad b = \frac{n_y}{n_x}h \qquad (3.2.13)$$

$$xin1 = x = x_i - b \qquad yin1 = y_j$$

$$xin2 = x_i \qquad yin2 = y = y_j - h$$

(c) case north-west

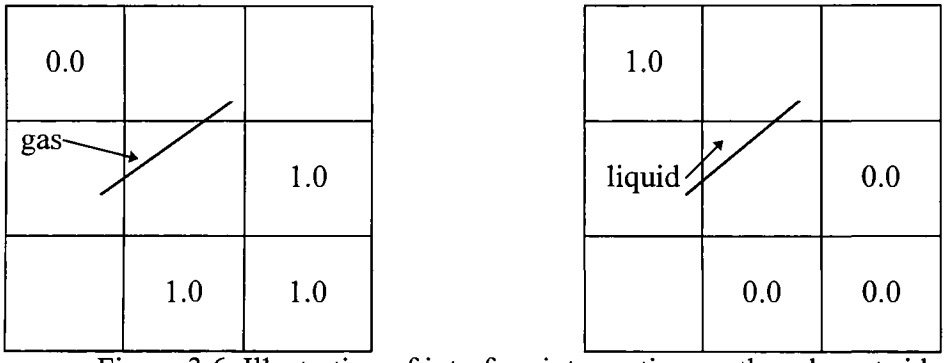

Figure 3.6: Illustration of interface intersecting north and west sides

$$n_x x + n_y y_j = d \qquad (3.2.14.a)$$

$$n_x x_{i-1} + n_y y = d \qquad (3.2.14.b)$$

(3.2.15.a)-(3.2.15.b): $n_x(x - x_{i-1}) + n_y(y_j - y) = 0$ (3.2.15)

Let $b = x - x_{i-1}$ and $h = y_j - y$

Thus, $n_x b + n_y h = 0$ (3.2.16)

$$\frac{b \cdot h}{2} = A \qquad (3.2.17)$$

where $A = (1 - f_{i,j})\,dx\,dy$ for gas (3.2.18.a)

and $A = f_{i,j}\,dx\,dy$ for liquid (3.2.18.b)

$$h = \sqrt{-2\frac{n_x}{n_y}A} \qquad b = -\frac{n_y}{n_x}h \tag{3.2.19}$$

$$xin1 = x_{i-1} \qquad yin1 = y = y_j - h$$

$$xin2 = x_{i-1} + b \qquad yin2 = y_j$$

(d) case south-west

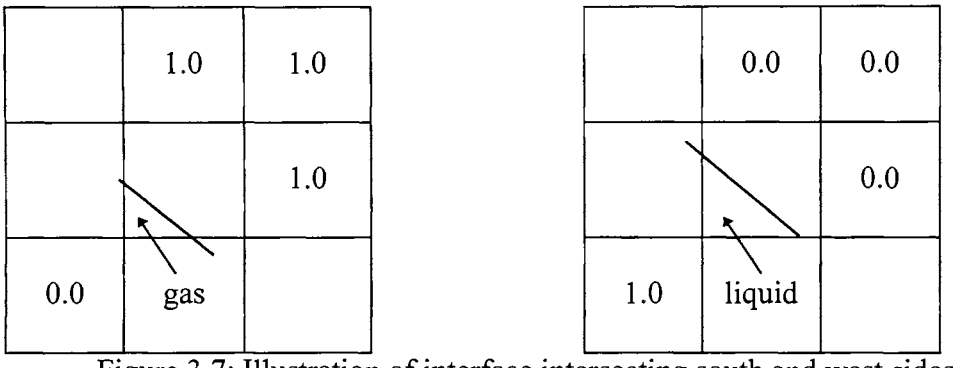

Figure 3.7: Illustration of interface intersecting south and west sides

$$n_x x_{i-1} + n_y y = d \tag{3.2.20.a}$$

$$n_x x + n_y y_{j-1} = d \tag{3.2.20.b}$$

(3.2.22.a)-(3.2.22.b): $n_x(x_{i-1} - x) + n_y(y - y_{j-1}) = 0$ (3.2.21)

Let $b = x - x_{i-1}$ and $h = y - y_{j-1}$

Thus, $-n_x b + n_y h = 0$ (3.2.22)

$$\frac{b \cdot h}{2} = A \tag{3.2.23}$$

where $A = (1 - f_{i,j})\,dx\,dy$ for gas (3.2.24.a)

and $A = f_{i,j}\,dx\,dy$ for liquid (3.2.24.b)

$$h = \sqrt{2\frac{n_x}{n_y}A} \qquad b = \frac{n_y}{n_x}h \qquad (3.2.25)$$

$$xin1 = x_{i-1} \qquad yin1 = y = y_{j-1} + h$$

$$xin2 = x = x_{i-1} + b \qquad yin2 = y_{j-1}$$

3.2.3 Case of the Interface Intersecting Opposite Sides

In the case where the interface intersects opposite sides, the interface line with the grid forms a trapezoidal area. The longest base is denoted by B and the shortest base by b.

(a) case east-west

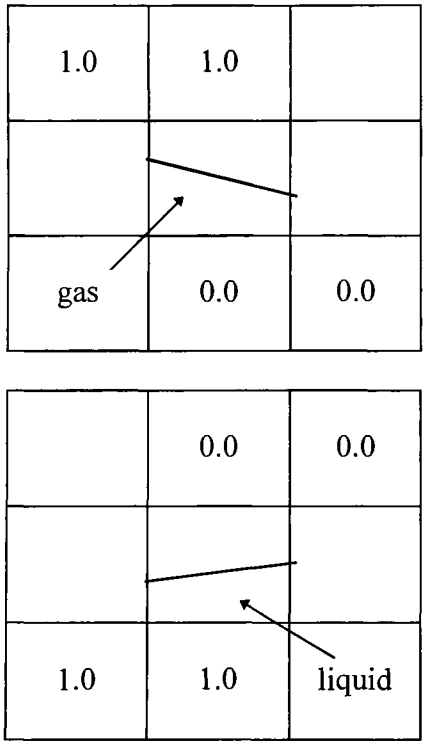

Figure 3.8: Illustration of interface intersecting east and west sides

The interface intersects the east side at $xin1 = x_{i-1}$, and the interface cuts the west side at $xin2 = x_i$. The interface line (Eq. 3.1.1) must pass through the two points of intersection:

$$n_x xin1 + n_y yin1 = d \tag{3.2.26.a}$$

$$n_x xin2 + n_y yin2 = d \tag{3.2.26.b}$$

(3.2.28.a)-(3.2.28.b): $n_x(xin1 - xin2) + n_y(yin1 - yin2) = 0$ (3.2.27)

Let $B = yin1 - y_{J-1}$ and $b = yin2 - y_{J-1}$,

Thus Eq. (3.2.27) becomes:

$$n_x(xin1 - xin2) + n_y(B - b) = 0 \tag{3.2.28}$$

Let A be the area of the trapezoid formed by the interface intersecting the east and west side.

$$A = \frac{(B+b)\cdot dx}{2} \tag{3.2.29}$$

where $A = (1 - f_{I,J})\,dx\,dy$ for gas (3.2.30.a)

and $A = f_{I,J}\,dx\,dy$ for liquid (3.2.30.b)

By solving Eq. (3.2.30) with Eq. (3.2.31), B and b are found.

$$B = \frac{A}{dx} - \frac{n_x}{2n_y}(xin1 - xin2) \tag{3.2.31}$$

$$b = \frac{A}{dx} + \frac{n_x}{2n_y}(xin1 - xin2) \tag{3.2.32}$$

And finally, $yin1 = B + y_{J-1}$ and $yin2 = b + y_{J-1}$

In a similar way, the intersection points where the interface intersects north south sides are determined.

(b) case north south

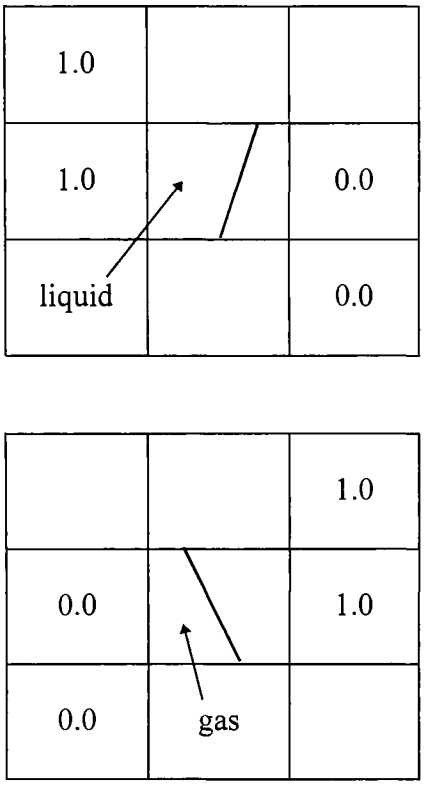

Figure 3.9: Illustration of interface intersecting north and south sides

$yin1 = y_{J-1}$ $\quad$ $yin2 = y_J$

$$n_x xin1 + n_y yin1 = d \tag{3.2.33.a}$$

$$n_x xin2 + n_y yin2 = d \tag{3.2.33.b}$$

(3.2.36.a)-(3.2.36.b): $n_x(xin1 - xin2) + n_y(yin1 - yin2) = 0$ (3.2.34)

Let $B = xin1 - x_{I-1}$ and $b = xin2 - x_{I-1}$

Thus,

$$n_x(B - b) + n_y(yin1 - yin2) = 0 \tag{3.2.35}$$

$$\frac{(B + b) \cdot dx}{2} = A \tag{3.2.36}$$

where $A = (1 - f_{i,j})\,dx\,dy$ for gas (3.2.37.a)

and $A = f_{i,j}\,dx\,dy$ for liquid (3.2.37.b)

$$B = \frac{A}{dx} - \frac{n_y}{2n_x}(yin1 - yin2) \qquad b = \frac{A}{dx} + \frac{n_y}{2n_x}(yin1 - yin2) \quad (3.2.38)$$

$$xin1 = B + x_{i-1} \qquad xin2 = b + x_{i-1}$$

To fix the problem of a bad interface reconstrution due to the smearing of f when f is calculated with the flow equations, f values less than $9x10^{-2}$ were set to 0, and f values greater than $1\text{-}9x10^{-2}$ were set to 1. Also redundant cases were eliminated by adding supplementary test on the f values.

3.3 Interface Reconstruction of Half a Circle

This section presents the interface reconstruction of half a circle on three different grid sizes: (1) 51x11, (2) 76x16 and (3) 101x21. The main purpose is to assess the numerical accuracy of the present technique while conducting grid refinement. The f values where initialized to represent the circular interface of half a circle. Figures 3.10, 3.11 and 3.12 show the piecewise linear interface reconstruction obtained.

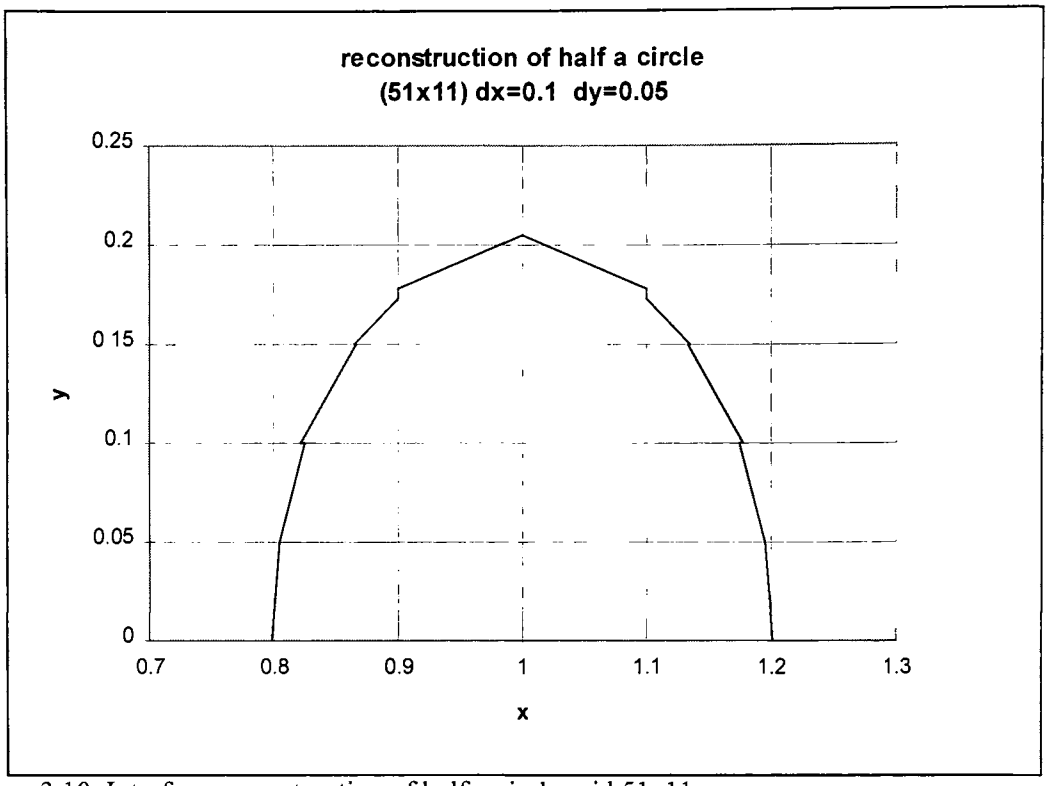

Figure 3.10: Interface reconstruction of half a circle grid 51x11

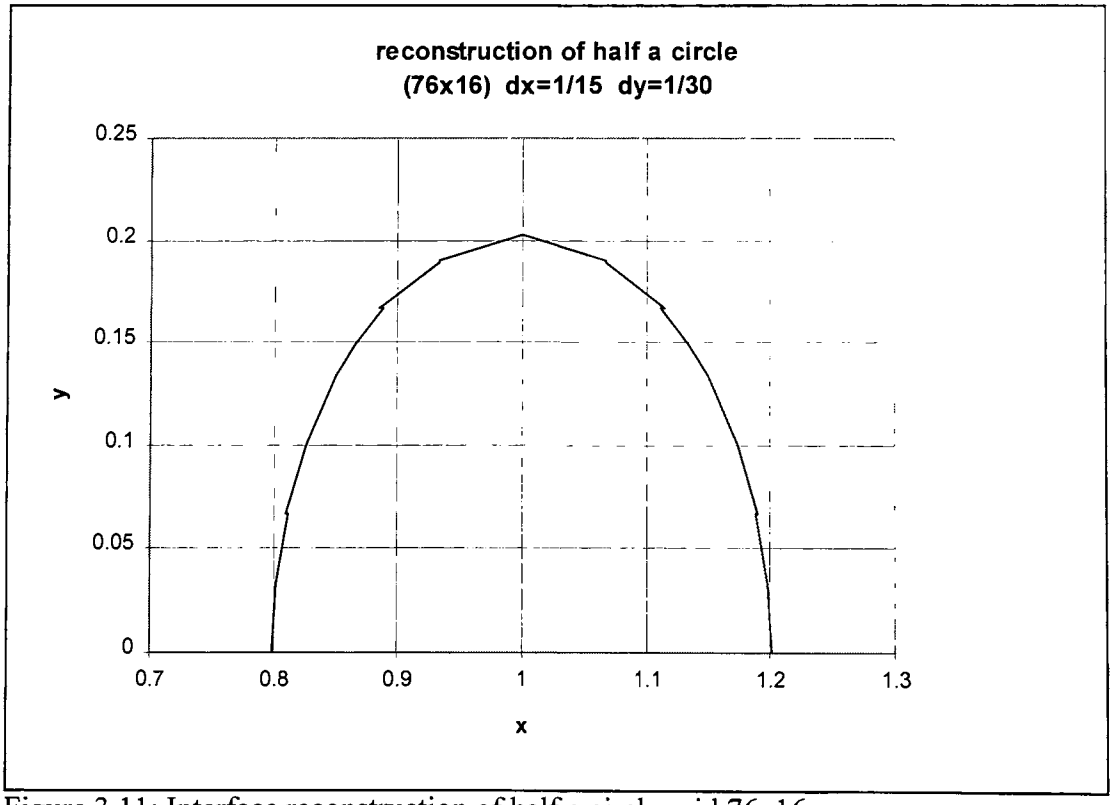

Figure 3.11: Interface reconstruction of half a circle grid 76x16

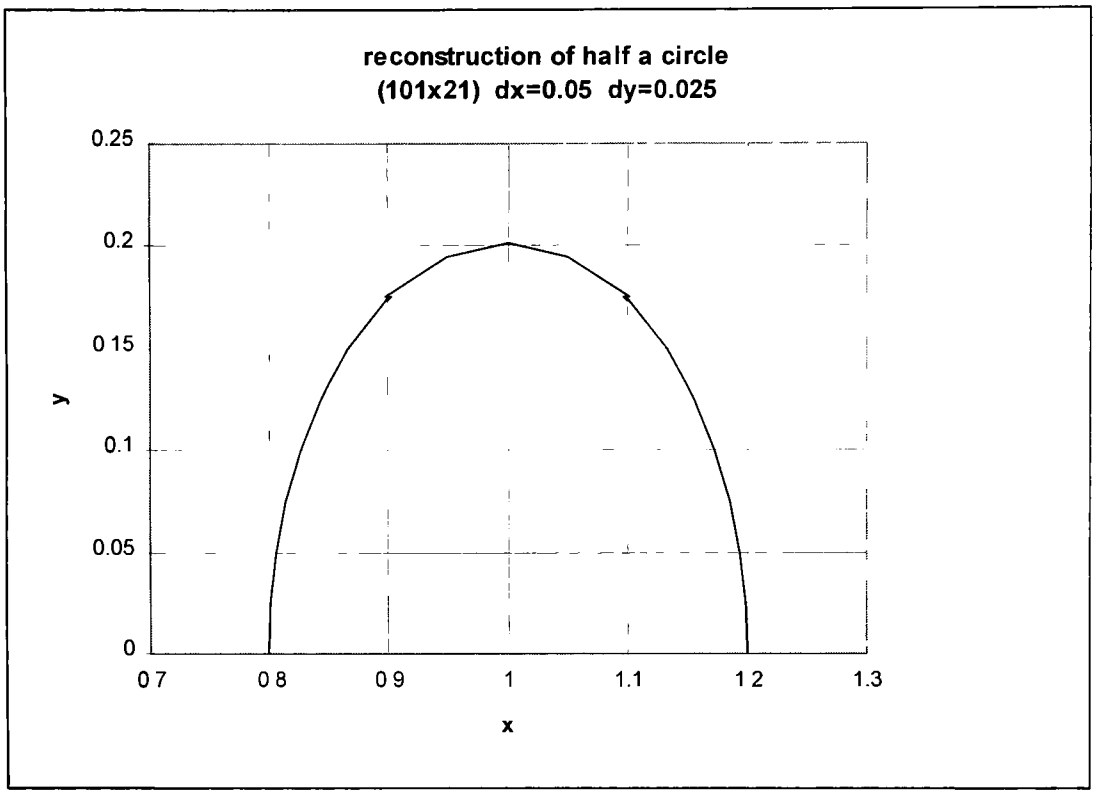

Figure 3.12: Interface reconstruction of half a circle grid 101x21

The error is calculated as:

$$error = \frac{\sum \varepsilon}{h} \qquad \text{Eq. (3.3.1)}$$

with h the number of location where ε is calculated as:

$$\varepsilon = \frac{\left| y_{exact} - y_{interface} \right|}{y_{exact}} \qquad \text{Eq. (3.3.2)}$$

Table 3.1: Comparison to the exact shape with the linear interface reconstruction on three different grid sizes

Grid	Error (%)
51x11	4.875
76x16	2.323
101x21	1.625

As expected, by increasing the precision of the grid, i.e., using a finer mesh, the error decreases.

3.4 Improvements of the linear approximation

One can improve the accuracy of the interface reconstruction by taking the midpoint of two intersection points located on the same grid line. In this manner the discontinuities encountered in the linear approximation are eliminated.

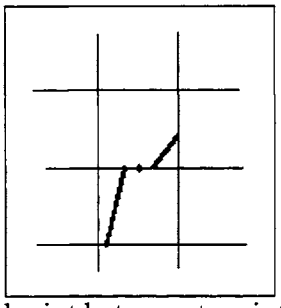

Figure 3.13: Midpoint between two intersection points

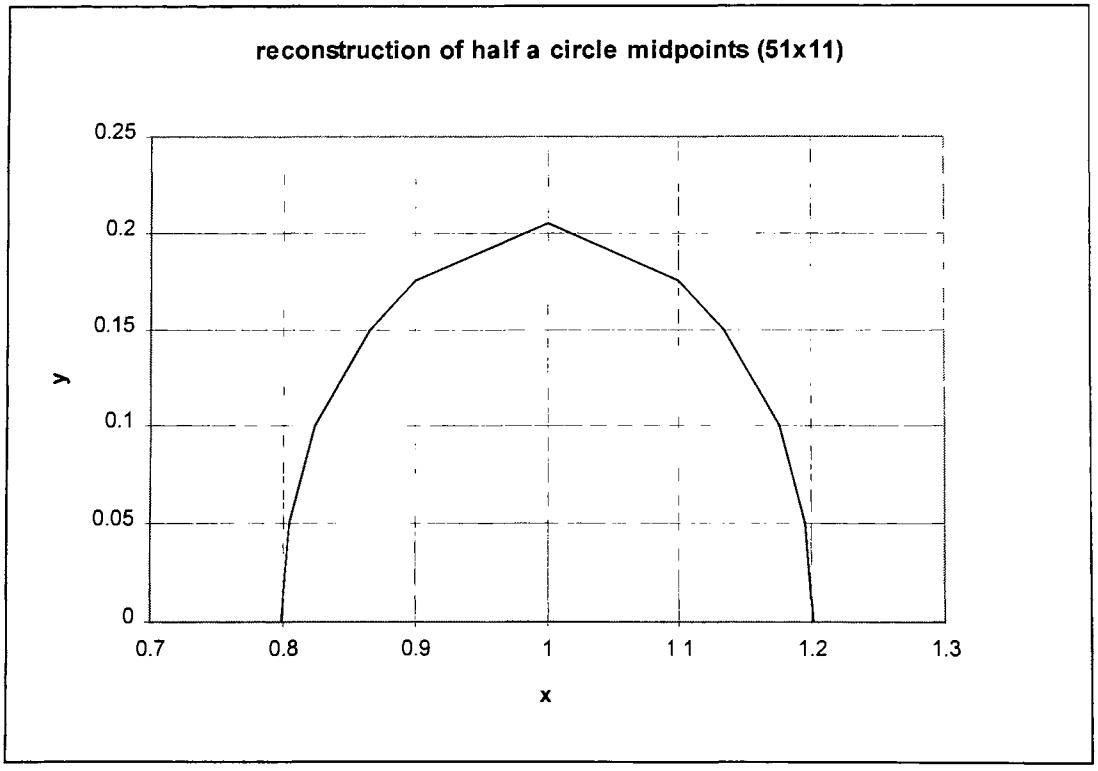

Figure 3.14: Interface reconstruction of half a circle using midpoints grid 51x11

Instead of using a straight line to connect the intersection points, one can use a polynomial curve. A cubic polynomial is used to model each segment between consecutive data points and the slope of each cubic polynomial is matched at the data points. This is realized by the MATLAB interpolation function "cubic spline". An interpolation between the midpoints (in1mp) was done and also between segment midpoints (in1ms). In this case, the interpolate curve is tangent to the linear segment joining the midpoints. Figure 3.15 presents the results of the two interpolations on the 51x11 grid. Table 3.2 presents the percentage error to the exact shape of the different improved interface reconstruction methods.

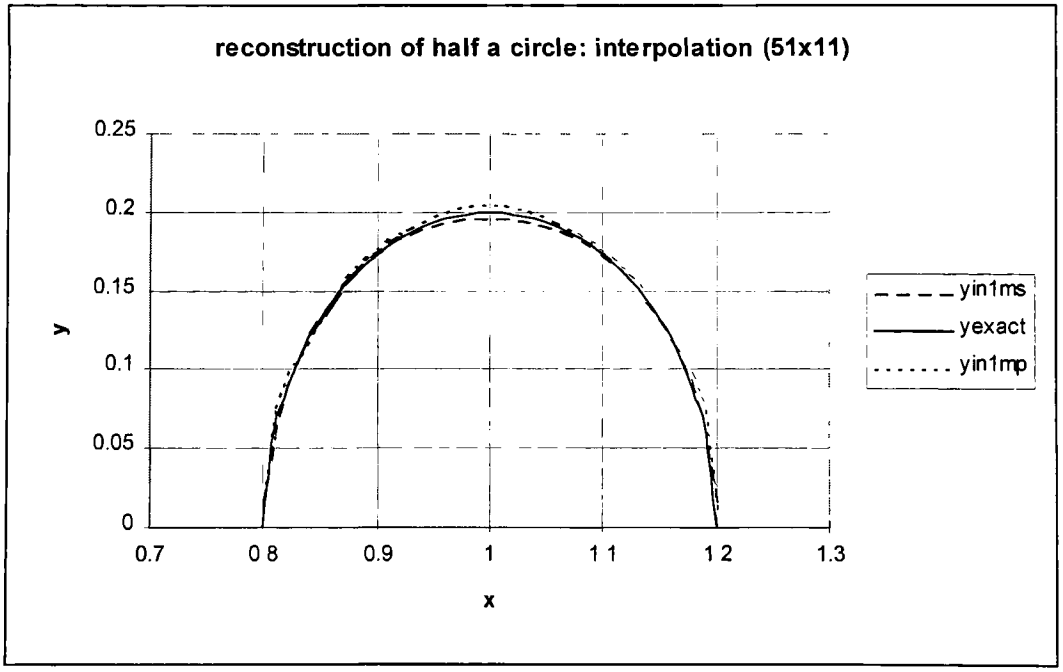

Figure 3.15: Interface reconstruction of half a circle using interpolation grid 51x11

Table 3.2: Comparison to the exact shape with the different interface reconstruction methods

Method	Error (%)
linear approximation	4.875
midpoints	4.672
inter. midpoints	2.939
inter. midsegments	1.206

By doing the interpolations in both ways, the precision is increased as shown in Table 3.2.

In summary, an interface reconstruction algorithm has been described in detail and methods of improvements have been demonstrated.

CHAPTER 4: CONVECTION OF A TWO-FLUID CHANNEL FLOW WITH A CYLINDRICAL INTERFACE

In order to demonstrate the capabilities of the code this chapter presents a problem in two dimensions of the convection of a two-fluid channel flow with a cylindrical interface.

4.1 Definition of the Problem

Two fluids, fluid 1 and fluid 2, are considered. The channel is filled with fluid 1. Fluid 2 is initially confined in a cylindrical domain with a circular cross-section at the entrance of channel. The center of the circurlar cross-section is on the symmetry axis of the channel. A constant velocity flow is given at the inlet of the channel. The outlet of the channel is open. The channel has a 5:1 length L to width l ratio (L/l=5). The cylindrical domain has a circular cross-section of diameter is 0.4 of the width ($0.4l$). The problem is described in Figure 4.1. The Reynolds number defined by Eq. 4.1.1 is equal to 10, and the Capillary number defined by Eq. 4.1.2 is 0.4. The density ratio between the two fluids. (ρ_2/ρ_1) is 1/2.

$$\mathrm{Re} = \frac{\rho_1 U l}{\mu_1} = \frac{inertia\ force}{viscous\ force} \tag{4.1.1}$$

with l the width of the channel, ρ_1 the density of fluid 1 and μ_1 the viscosity of fluid 1.

$$Ca = \frac{\mu_1 U}{\sigma} = \frac{viscous\ force}{capillary\ force} \tag{4.1.2}$$

with σ the surface tension.

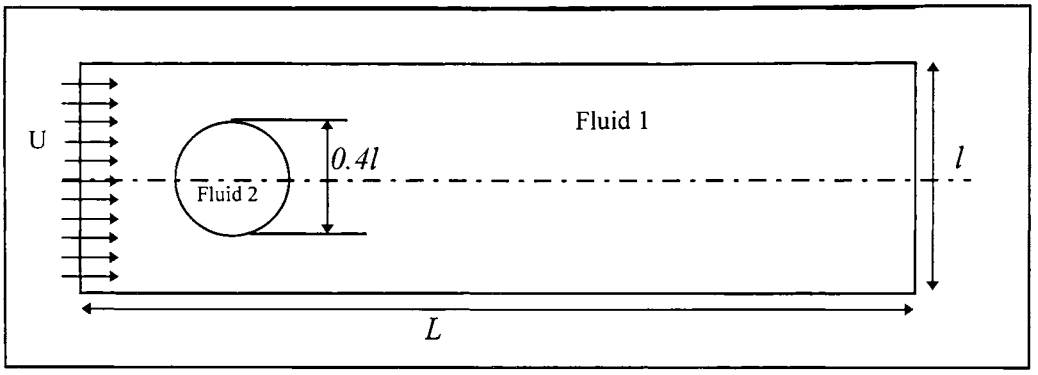

Figure 4.1: Description of the Problem

Boundary Conditions

- at the wall, the no-slip condition gives:

$$u = 0 \quad v = 0 \tag{4.1.3}$$

- since the problem is symmetric, only half of the domain is necessary to be considered, and the following conditions can be applied on the symmetry axis of the channel:

$$\frac{\partial u}{\partial x} = 0 \qquad v = 0 \tag{4.1.4}$$

- at the inlet

$$u = U \qquad v = 0 \tag{4.1.5}$$

- at the outlet

$$\frac{\partial u}{\partial x} = 0 \quad \frac{\partial v}{\partial x} = 0 \tag{4.1.6}$$

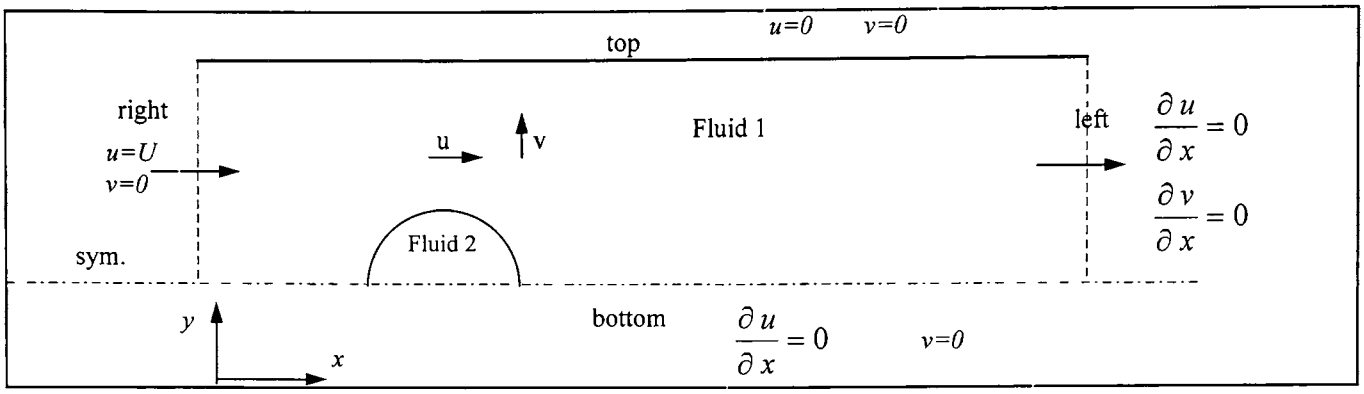

Figure 4.2: Boundary conditions

Grids

Three different uniform grids have been used to solve the problem.

(1) 51 x 11

(2) 76 x 16

(3) 101 x 21

Time Step

Δt is chosen to satisfy the convection stability criteria:

$$\Delta t \leq 0.2 \frac{\Delta x}{\max u} \qquad (4.1.7)$$

Initial Configuration

At t=0s, the bubble of radius 0.2 is centered at x=1 as shown in Figure 4.3.

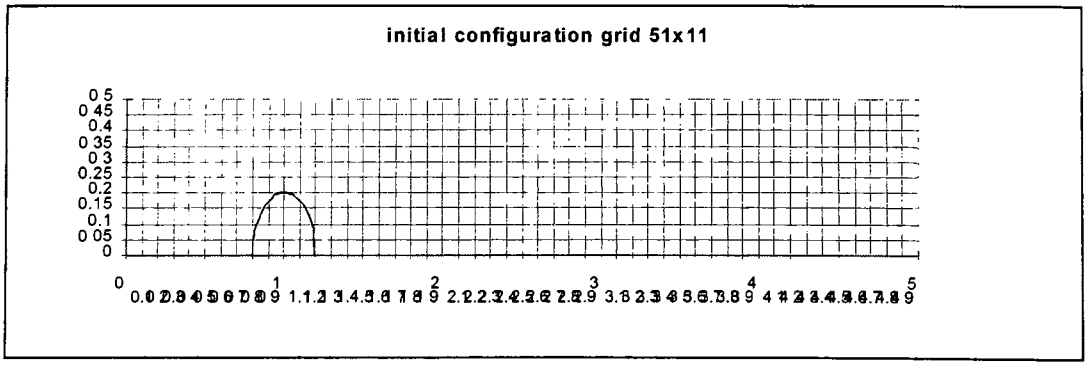

Figure 4.3: Initial Configuration

4.2 Results

4.2.1 at t=0.5s

At t=0.5s, the bubble is stretched to the right of the channel as it can be observed in Figures 4.4, 4.5 and 4.6 for the grid 51x11, 76x16, and 101x21, respectively.

At t=0.5s, the mass conservation of the bubble is verified. For the 51x11 grid, the mass is conserved with an error of 0.146%, for the 76x16 grid, the error is 0.0055%, and for the 101x21, grid the error is 0.0051%.

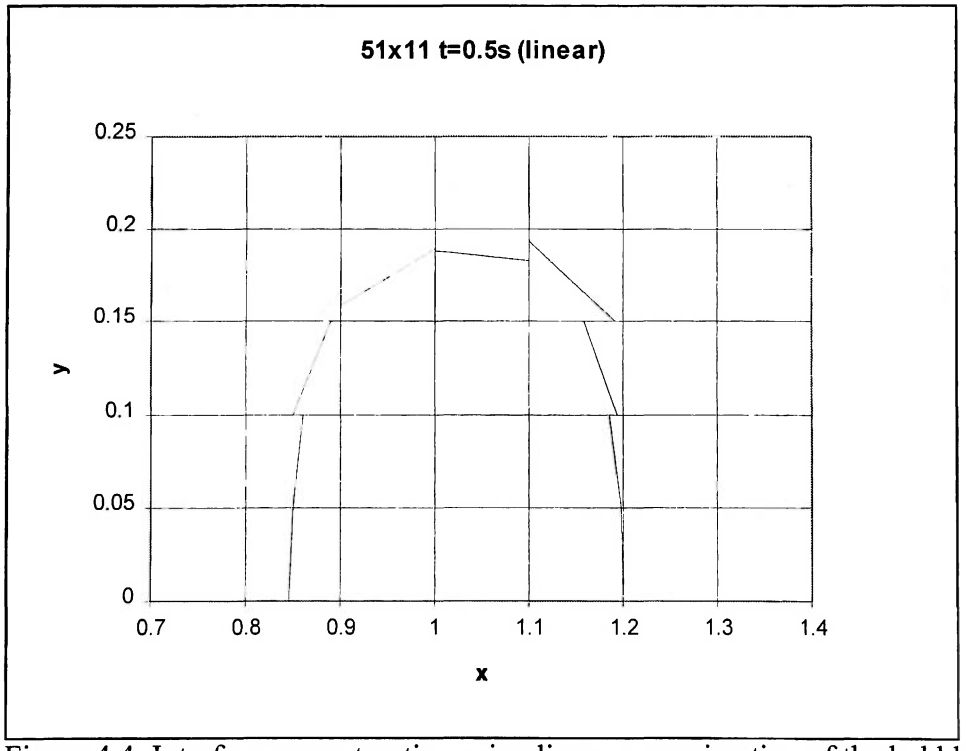

Figure 4.4: Interface reconstruction using linear approximation of the bubble at t=0.5s grid (51x11)

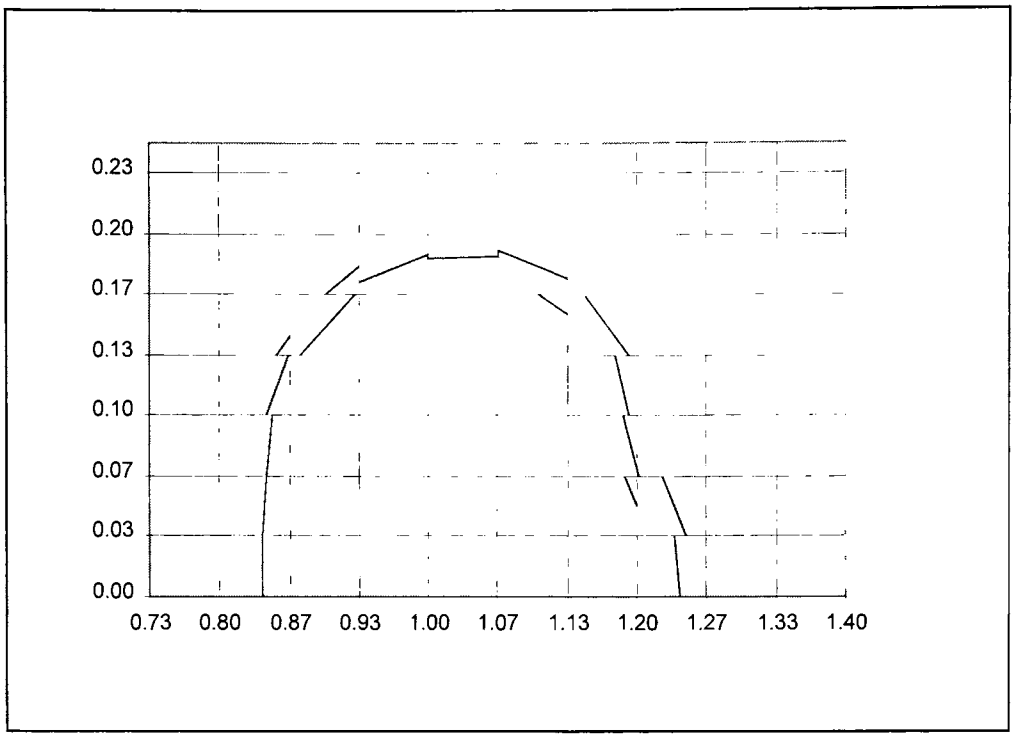

Figure 4.5: Interface reconstruction using linear approximation of the bubble at t=0.5s grid (76x16)

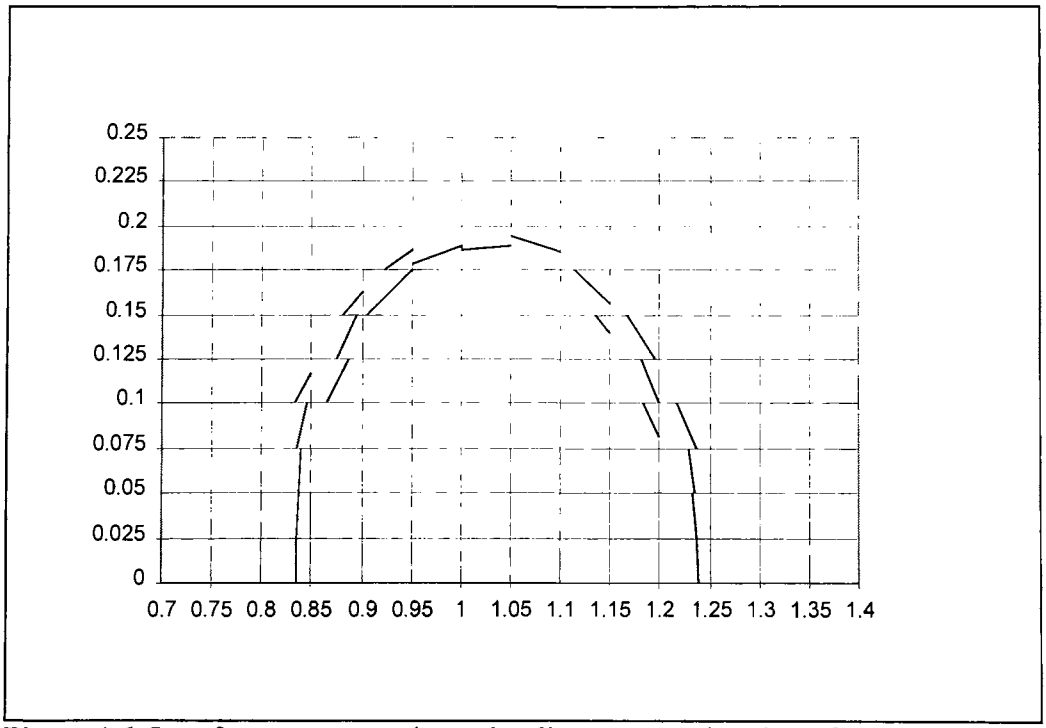

Figure 4.6: Interface reconstruction using linear approximation of the bubble at t=0.5s grid (101x21)

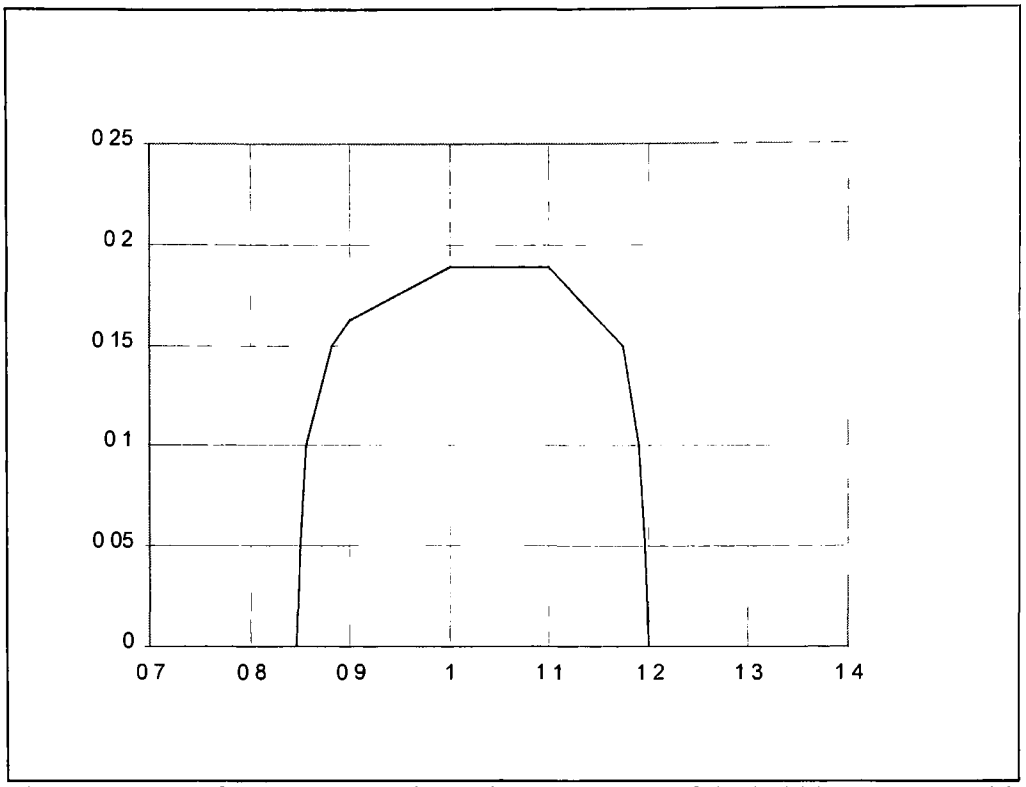

Figure 4.7: Interface reconstruction using midpoints of the bubble at t=0.5s grid (51x11)

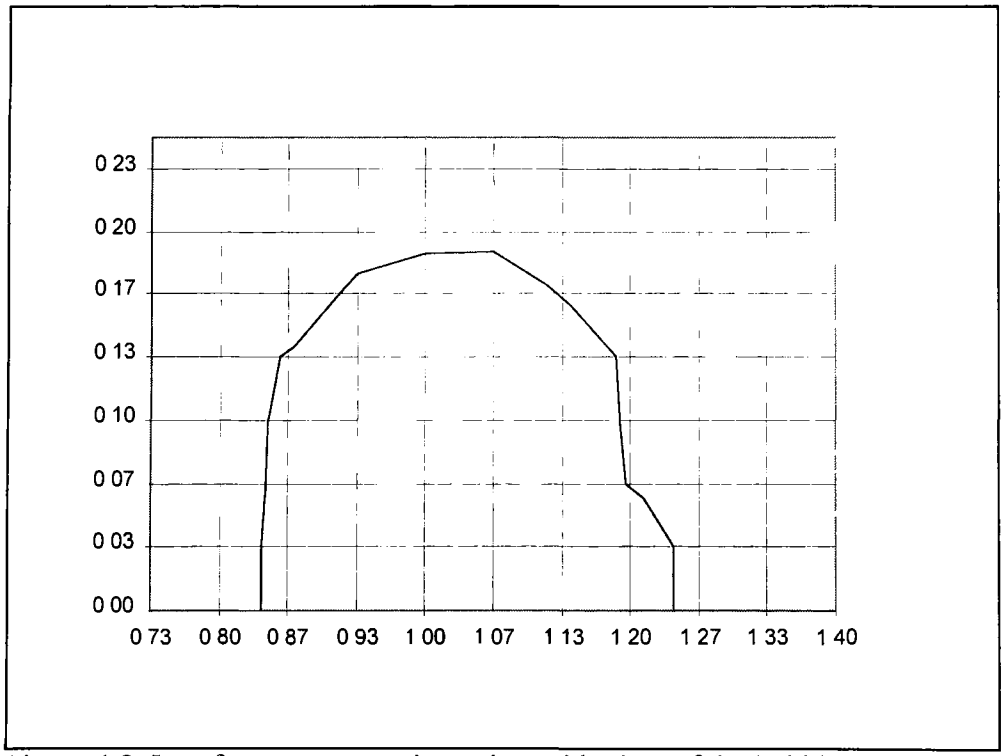

Figure 4.8: Interface reconstruction using midpoints of the bubble at t=0.5s grid (76x16)

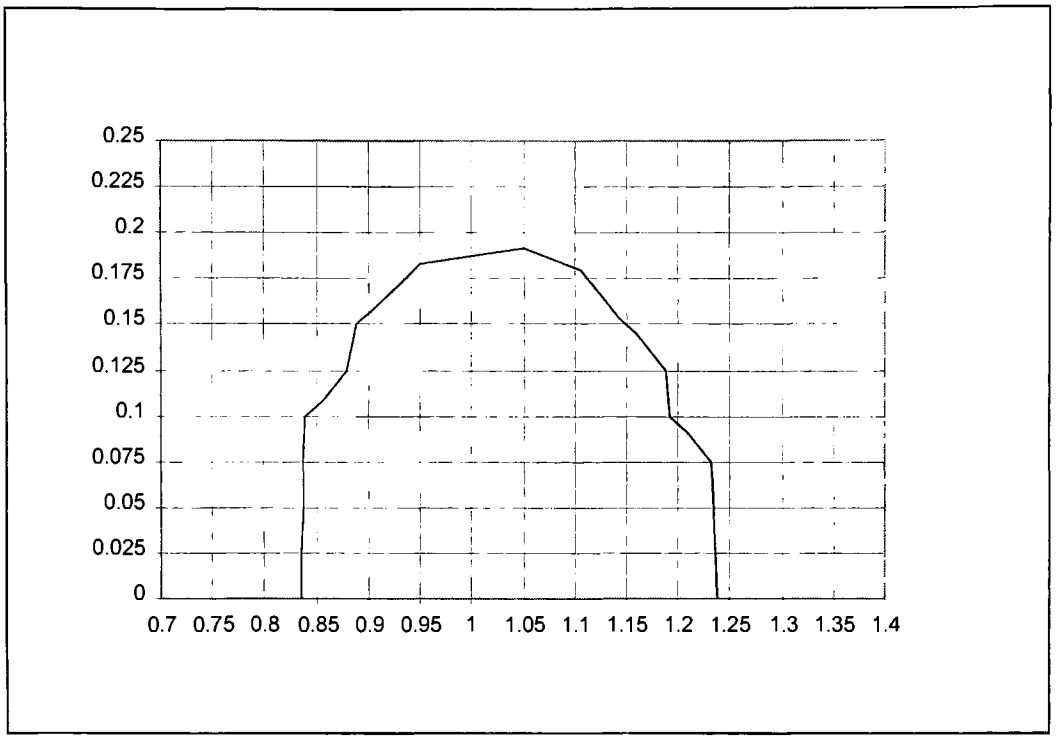

Figure 4.9: Interface reconstruction using midpoints of the bubble at t=0.5s grid (101x21)

The velocity vectors are presented in Figure 4.10 and the streamlines in Figure 4.11.

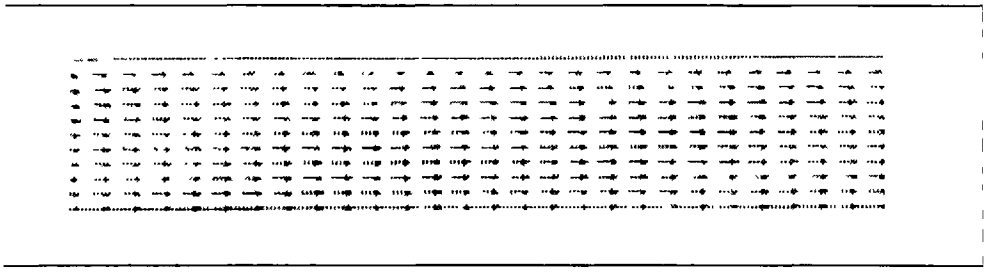

Figure 4.10: Velocity vectors at t=0.5s grid 51x11 (zoom view)

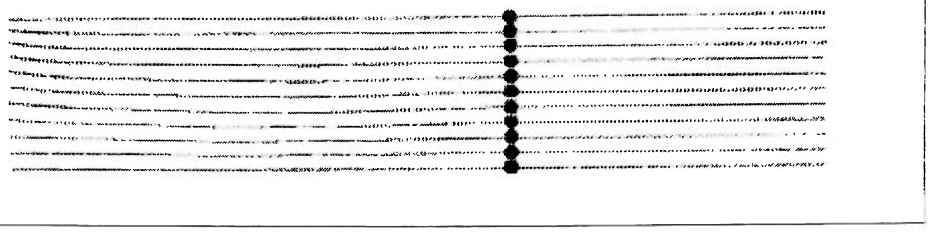

Figure 4.11: Streamlines at t=0.5s grid 51x11 (zoom view)

4.2.2 at t=2s

The velocity vectors and streamlines are plotted in Figure 4.12 and 4.13.

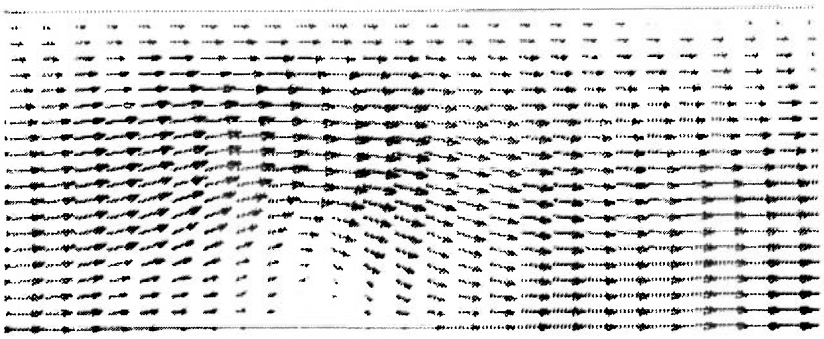

Figure 4.12: Velocity vectors at t=2s grid 101x21 (zoom view)

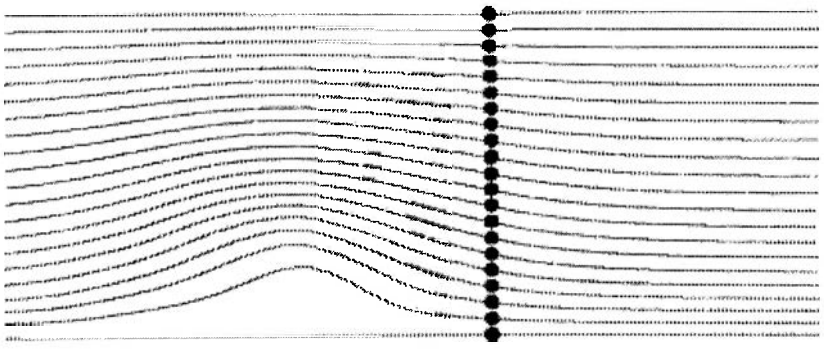

Figure 4.13: **Streamlines at** t=2s **grid** 101x21 (zoom view)

CHAPTER 5: CONCLUSION AND RECOMMENDATIONS

In this work, the volume of fluid method was investigated for moving boundary problems and a computational implementation has been developed.

5.1 Accomplishements

1. The Volume of fluid method was combined with the Continuum surface force model. The governing flow equations for Newtonian fluids in incompressible flows in two dimensions were solved using the pressure based Patankar's algorithm.

2. A linear interface reconstruction algorithm was developed to improve the accuracy of the interface definition.

3. The code was tested to solve the problem of the convection of a spherical bubble in a channel. From this, it was demonstrated that the volume of fluid method is well suited to solve moving boundary problems if the accuracy requirement of the interface definition is not stringent. The current limitation of the volume of fluid method is the problem of the smearing of the volume of fluid fraction f, and the resulting discontinuity in interface shapes and/or slopes.

5.2 Recommendations for future work

One can improve the interface reconstruction by developing an algorithm that considers a higher order polynomial instead of a straight line. By doing this it will be necessary to update the surface force $\vec{F}_{sv}$ at every calculation since the normal to the interface will have been modified. The present code can also be improved by inserting a volume of fluid method advection algorithm. The volume of fluid fraction function f can be viewed as a representation of a given fluid type, and it will be transported by convection and diffusion (if included) to indicate the movement of the fluid.

REFERENCES

Ashgriz N. and Poo J.Y., 1991, "FLAIR: Flux Line-Segment Model for Advection and Interface Reconstruction", *Journal of Computational Physics*, Vol. 93, pp.449-468

Brackbill J.U., Kothe D.B., and Zemach C., 1992, "A Continuum Method for Modeling Surface Tension", *Journal of Computational Physics*, Vol. 100, pp.335-354

Floryan J.M., Rasmussen H., 1989, "Numerical Methods for Viscous Flows with Moving Boundaries", *Appl. Mech. Rev.*, Vol. 42, No. 12, pp. 323-340

Hirt C.W. and Nichols B.D., 1981, "Volume of Fluid (VOF) Method for Dynamics of Free Boundaries", *Journal of Computational Physics*, Vol. 19, pp.201-225

Kothe D.B. and Mjolness R.C., 1992, "RIPPLE: A New Model for Incompressible Flows with Free Surfaces", *AIAA Journal*, Vol. 30, No. 11, pp. 2694-2700

Kothe D.B. and Rider W.J., 1994, "Comments on Modeling Interfacial Flows with Volume of Fluid Methods, *Los Alamos Scientific Laboratory Report,* LA-UR-94-3384, Los Alamos, NM

Liang 1991, "Numerical Method for Calculation of Surface Tension Flows in Arbitrary Grids", *AIAA Journal*, Vol. 29, No. 2, pp. 161-167

Mack K., Bugg J.D., and Rezkallah K.S., 1995, "Numerical Simulation of Bubbly Flow Under Reduced Gravity Conditions", *Proceedings of the 6th International Symposium of Computational Fluid Dynamics, Lake Tahoe, Nevada*, pp. 750-755

Nichols B.D. Hirt C.W. and Hotchkiss R.S., 1980, "SOLA-VOF: A Solution Algorithm for Transient Fluid Flow with Multiple Free Boundaries", *Los Alamos Scientific Laboratory Report*, LA-8355

Patankar S.V. 1980, "Numerical Heat Transfer and Fluid Flow", Hemisphere, Washington D.C.

Shyy W.,1994, "Computational Modeling for Fluid Flow and Interfacial Transport", Elsevier Science Publishers B.V.

Shyy W., Thakur S., and Wright J., 1992, "Second-Order Upwind and Central Difference Schemes for Recirculating Flow Computation", *AIAA Journal*, Vol. 30, No. 4, pp. 923-932

Shyy W., Udaykumar H.S., Rao M.M., Smith R.W., 1996, Computational Fluid Dynamics with moving Boundaries, Taylor & Francis

Tomiyama A., Sou A., and Sakaguchi T., 1996, " Numerical Simulation of a Taylor Bubble in a Stagnant Liquid inside a Vertical Pipe", *JSME International Journal, Series B*, Vol. 39, No. 3,pp. 517-5241

Udaykumar H.S., Kan H.C., Shyy W. and Tran-Son-Tray R., "Multiphase Dynamics in Arbitrary Geometries on Fixed Cartesian Grids".

Youngs D.L., 1984,"Time-Dependent Multi-Material Flow with Large Fluid Distorsion", in K.W. Morton and M.J. Baines (eds.), *Numerical Methods for Fluid Dynamics*, Academic Press, New York, pp. 273-285

APPENDIX 1: FLOW CHART OF THE PROGRAM ENVOF